


## Research Article

# Time-Series Forecasting of a Typical PWR Undergoing Large Break LOCA

Michal Kaminski<sup>1</sup> and Aya Diab<sup>1,2</sup> 

<sup>1</sup>Department of NPP Engineering, KEPCO International Nuclear Graduate School, Ulsan, Republic of Korea

<sup>2</sup>Mechanical Power Engineering Department, Faculty of Engineering, Ain Shams University, Cairo, Egypt

Correspondence should be addressed to Aya Diab; [aya.diab@gmail.com](mailto:aya.diab@gmail.com)

Received 13 June 2023; Revised 16 January 2024; Accepted 14 February 2024; Published 8 March 2024

Academic Editor: Doddy Kastanya

Copyright © 2024 Michal Kaminski and Aya Diab. This is an open access article distributed under the Creative Commons Attribution License, which permits unrestricted use, distribution, and reproduction in any medium, provided the original work is properly cited.

In this work, a machine learning (ML) metamodel is developed for the time-series forecasting of a typical nuclear power plant response undergoing a loss of coolant accident (LOCA). The plant model of choice is based on the APR1400 nuclear reactor. The key systems and components of APR1400 relevant to the investigated scenario are modelled using the thermal-hydraulic code, RELAP5/MOD3.4, following the description published in the design control document. The model is tested under a spectrum of initial and boundary conditions via propagation of key uncertain parameters (UPs) which are derived from the phenomena identification and ranking table (PIRT). This is achieved by loosely coupling RELAP5/MOD3.4 with the statistical tool, Dakota. The most probable nuclear power plant (NPP) response was calculated using the best estimate plus uncertainty (BEPU) approach. Next, the database generated from the NPP system response was used as an input for the ML model. The NPP system response was represented by peak cladding temperature (PCT), safety injection system (SIT), mass flow rate, reactor power, and primary system pressure. In this research, two regression models were tested with reasonably good performance, namely, the gated recurrent unit (GRU) and the long short-term memory (LSTM).

## 1. Introduction

Modern nuclear power plants (NPPs) are developed with safety as the main priority. During normal operation, operators in the main control room (MCR) continuously monitor a myriad of nuclear power plant (NPP) parameters in order to keep them within their nominal conditions. Under accident conditions, MCR operators should comprehend the current plant dynamics in real time. This includes accident diagnosis following an emergency situation for which timing and precision are key to the decision-making process to keep the NPP safe.

However, under accident conditions, the operators are exposed to stressful conditions and may need to take timely decisions. To expedite the decision-making process and simultaneously minimize the possibility of human error, a machine learning (ML) prediction model is proposed using a multistep artificial neural network. The ML model is

trained to mimic the most NPP system response generated using a physics-based model for a set of initial, operating, and boundary conditions. The main goal of this research is to develop a machine learning (ML) model for real-time prediction of NPP response under accident conditions to help operators in the MCR expedite the decision-making process [1]. Some of the most challenging conditions for the operators are the loss of coolant accident (LOCA) or an extended station blackout (SBO). Under those conditions, a core meltdown may be potentially inevitable if the ultimate heat sink is completely lost [2]. In case of LOCA, the loss of ultimate heat sink may be due to the unavailability of the emergency core cooling system. While for SBO, this may be due to the loss of the heat removal system as evidenced by the Fukushima Daiichi accident. In this research, a large break loss of coolant accident (LBLOCA) is considered as a bounding scenario for design basis accidents.

ML is actively being sought for the development of digital twins [3] for preventive maintenance, as well as the autonomous control of nuclear power plants in an attempt to minimize the possibility of human errors [4]. For example, an ML model has been developed by implementing an artificial neural network (ANN) along with the back-propagation algorithm to help in mitigating a loss of feedwater (LOFW) accident in a multiapplication small light water reactor [5]. A fast-running model conditional autoencoder (CAE), known as an auto-associative neural network (AANN), can predict the pressure as well as peak cladding temperature (PCT) in APR1400 under a small break LOCA (SBLOCA) scenario [6]. Similarly, an ANN model that can also support the implementation of the diverse and flexible coping strategy (FLEX) has been developed for an extended SBO [7, 8]. Prediction of the peak cladding temperature (PCT) and influence of the FLEX strategy for APR1400 undergoing an extended station blackout (SBO) was performed using an artificial neural network (ANN) [9]. Usage of artificial neural networks (ANNs) such as deep learning neural networks (DLNNs) and convolutional neural networks (CNNs) have been explored to predict the critical heat flux (CHF) of water flowing in reactor vessel channels [10, 11] without solving the underlying physics. Similarly, deep CNN and support vector regression (SVR) models were used to predict the core power distribution, reducing the time needed for such an operation while maintaining high accuracy [12, 13]. SVR has been used for fast and accurate reactor core loading pattern modelling [14]. ANN algorithms such as Kohonen self-organizing map, K-means, and Fuzzy C-means can be useful tools for flow pattern identification in tubes filled with the gas-liquid mixture [15]. In the wake of the accident at the Fukushima Daiichi, NPP researchers explored the use of codes such as MELCOR and MAAP to simulate the core behaviour under severe accident conditions and use the generated databases to develop and train ML models capable of predicting the NPP response at a fraction of the time needed using conventional methods and hence serving as an aiding tool for the decision-making process [16].

ML models have also been used to predict the diffusion and transport of radioactive materials in the atmosphere [17, 18] and the prediction of the radioprotector compounds' effectiveness and toxicity [19]. Furthermore, IAEA is supporting the increasing trend of using robots in environments contaminated with radiation [20]. Robots with a sophisticated level of artificial intelligence can help with general maintenance, decontamination, and postaccident activities such as search and rescue in NPPs [21].

Since accident prevention is a topmost priority for MCR operators, Korea Hydro and Nuclear Power Co., Ltd. (KHNP) developed an early warning system at the headquarters in Gyeongju. The system monitors and diagnoses 24 nuclear power plants in real time and uses ML to detect slight fault symptoms of equipment in advance, which allows the operators to prevent or prepare for failure and hence minimize losses caused by unplanned maintenance [22]. Currently, engineers from the Central Research Institute (CRI) KHNP are working on developing an ML model to

predict the NPP response under accident conditions. Faulty solenoid-operated valve (SOV) can be detected by AI using DNN and XGBoost regressor, as well as the emergency diesel generator (EDG) using CNN autoencoder by loading the sound waveform and spectrogram to the model [23, 24]. The program will detect the defective frequency and report the state of the tested device. Similarly, CNN can be used for crack detection on reactor vessel (RV) surfaces [25]. Early identification of potential material failure can prevent an accident in the future.

A wide variety of artificial intelligence (AI) applications in specific areas of the NPP system can help the MCR operators benefit from an accurate prediction of the NPP's system response during normal conditions like load following operation [26] or even add an extra level of protection when the NPP is experiencing an accident condition. ANN-based algorithms can diagnose and identify the accident scenario that the NPP is currently undergoing and predict the future system parameters based on the system response or operator's actions [5, 27].

Given the potential benefits of AI at large and specifically of machine learning (ML), this study builds on the work of Sallehuddin and Diab [28] and follows the work of Radaideh [29] to develop a time-series forecasting ML model capable of predicting the NPP real-time response for APR1400 undergoing an LBLOCA. Unlike the work of Sallehuddin and Diab [28], the NPP response is predicted as a function of time rather than pointwise prediction of a characteristic safety criterion. Furthermore, the current work is considered an extension of the earlier work of Radaideh [29] whose work focused on small break LOCA. The underlying physics with heterogeneous versus homogeneous vessel conditions is quite different. In the long term, the RCS will remain at high pressure for SB-LOCA and the injection flow rate is too low for effective cooling; thus, small breaks require cooling of the RCS by the SGs until shutdown cooling (SDC) can be initiated. On the other hand, under LBLOCA, the plant is adequately cooled by the injection flow because this flow is large due to the low RCS pressure.

To achieve this goal in an efficient and systematic manner, the work breakdown structure involved three building blocks. First, a thermal-hydraulic model of APR1400 undergoing an LBLOCA scenario was developed using RELAP5/MOD3.4. This was followed by the development of an uncertainty quantification framework using the DAKOTA platform to sample and propagate various uncertain parameters into the thermal-hydraulic model. A python script allows the communication and data exchange between the two codes, hence facilitating the automation of the sampling and propagation processes for the best estimate plus uncertainty analysis until a statistically representative sample size achieved. Once the database of possible system responses is generated, it is passed to the machine learning (ML) model for training and tuning with the ultimate goal of predicting key system responses. Given the nature of the problem, a time-series forecasting model based on recurrent neural network was selected. Specifically, the long-short-term memory (LSTM) and the gated recurrent unit (GRU) were compared.

## 2. Methodology

This section describes the methodology applied in this work, which involves three basic steps, namely, the development of a thermal-hydraulic model, an uncertainty quantification framework, and a machine learning model. For the machine learning model to predict the NPP response, it is necessary to generate a large enough database using the thermal hydraulics model, which in turn is driven by the uncertainty quantification framework as illustrated in Figure 1.

**2.1. Thermal-Hydraulics Model.** The thermal-hydraulics model is developed in RELAP5/MOD3.4 system code to simulate the nuclear power plant response under LBLOCA conditions [28]. The plant of choice for the analysis is the Korean Advanced Pressurized Reactor (APR1400). APR1400 is a cutting-edge nuclear power plant which evolved by upgrading and optimizing its predecessor, the OPR1000 power plant model. The design of APR1400 has been strengthened to satisfy the 0.3 g seismic requirements. In addition, the quadrant layout design of auxiliary building enhances its coping capabilities against extreme external events such as fire, flood, and earthquake. In 2019, APR1400 successfully achieved the Design Certification from the US Nuclear Regulatory Commission (NRC) and was successfully exported to UAE. More recently, the EU-APR, which is an evolutionary model of APR1400, received the European Utility Requirements (EURs) Certification.

LBLOCA is a hypothetical accident leading to the loss of the reactor coolant at a rate exceeding the capability of the reactor coolant makeup system. Generally speaking, a break involves a spectrum of sizes and locations; but according to the APR1400 design control document (DCD), the most limiting break is a 100 percent of a double-ended guillotine break at the largest pipe of the reactor coolant system (RCS), i.e., the pump discharge leg, which is the adopted assumption in the current work.

Under LBLOCA, the emergency core cooling water is delivered directly into the upper annulus of the reactor pressure vessel (RPV) via the direct vessel injection (DVI) nozzle. The innovative design of APR1400 involves a fluidic device (FD) to regulate the amount of injection flow from the safety injection tanks (SITs) depending on the phases of accident progression. The SITs in conjunction with the FD deliver high- and low-flow injections, which are equivalent to the conventional safety injection tank (accumulator) flow and low-pressure safety injection pump flow, respectively. After the safety injection tanks are depleted, the high-pressure safety injection pumps take over to ensure the emergency core cooling is achieved.

For the long-term cooling of the plant, the operator can initiate a controlled system cooldown by using the auxiliary feedwater (AFW) system in conjunction with the atmospheric dump valves (ADVs). In the absence of a forced reactor coolant flow, the RCS heat is removed by natural circulation along with the steam generators (SGs). After the reactor coolant temperature and pressure have been reduced to approximately 176.7°C and 31.6 kg/cm<sup>2</sup>, respectively, the

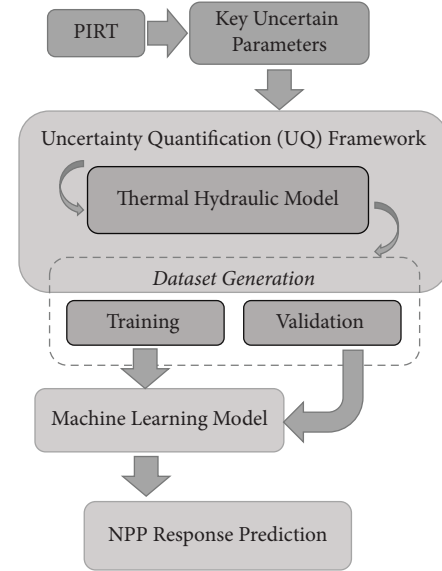


FIGURE 1: Data processing flowchart.

shutdown cooling system (SCS) is activated to reduce the RCS temperature to the cold shutdown condition. The cooldown capacity of the auxiliary feedwater system provides reasonable assurance that the shutdown cooling entry condition is reached before 8 hours.

The source of safety injection water is the IRWST and given the fact that it is located within the containment, simultaneously acting as a containment sump, the need for a switchover to recirculation mode is not applicable to the APR1400. The elimination of the ECCS realignment operator action is considered a significant improvement in the design of APR1400.

However, it is worth noting that for conservatism in safety analyses, such safety-related operator action is not credited for the mitigation of postulated events until 30 minutes after the event initiation even though the action can be performed from the main control room (MCR) within 30 minutes. Since the current work focuses on the short-term NPP response under LBLCA conditions, operator actions are not credited following the conservative safety analysis approach and consistent with APR1400 DCD.

To reflect the details of APR1400, the nodalization shown in Figure 2 contains the key systems and components. On the primary side, the reactor coolant system (RCS) with a reactor pressure vessel (RPV), two hot legs, four cold legs, four reactor circulating pumps (RCPs), a pressurizer (PRZ), and two steam generators (SGs) along with main steam lines and safety valves are represented using appropriate thermal-hydraulics components. The core inlet and outlet nozzles, downcomer, and lower and upper plenums as part of the reactor vessel are modelled as well. The reactor core is represented using an average channel and a hot channel, each is discretized using 20 vertical nodes.

The emergency core cooling system (ECCS) of the APR1400 is represented by modelling the safety injection system (SIS) and connected to the RPV at the upper annulus. The SIS contains the following two main components: four

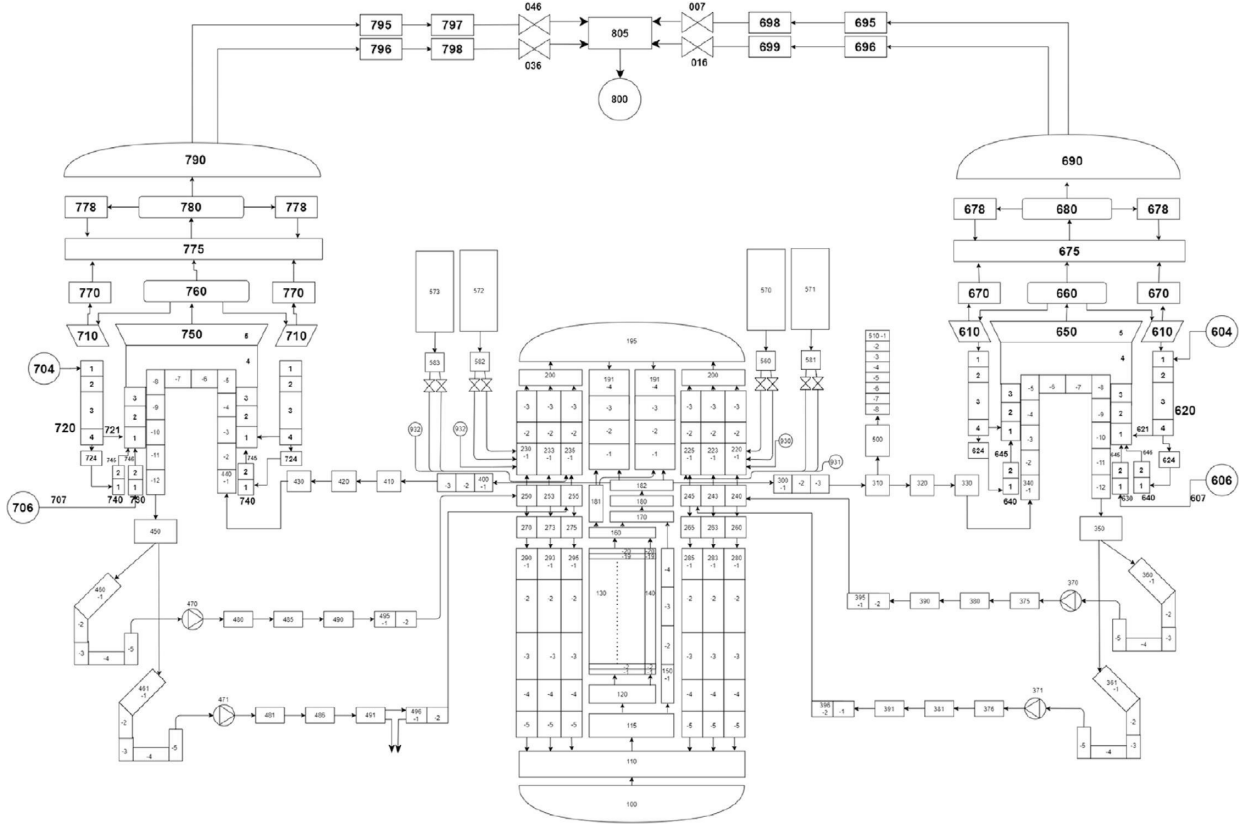


FIGURE 2: APR1400 nodalization for the LBLOCA thermal-hydraulic model [28] (reproduced from Sallehuddin and Diab, 2021, under the creative commons attribution license/public domain).

safety injection tanks (SITs) and four safety injection pumps (SIPs). Automatic operation of the SIPs is actuated by a low pressurizer pressure signal or a high containment pressure signal. In accordance with the conservative assumption of APR1400 design control document (DCD) for LBLOCA evaluation, two out of four SIPs are available during the accident to minimize the safety injection available to cool the core. However, with concurrent LOOP, the available SIPs (with a design temperature of 177°C) cannot start until the EDG startup and load sequencing. Hence, a time delay of 40 seconds is assumed after the safety injection actuation signal (SIAS) setpoint is reached. Flow is initiated from the SITs when the check valves open as the pressure in the RPV downcomer drops below the SIT pressure setpoint ( $\sim 4.25$  MPa).

The LBLOCA is activated at time zero with a doubled-ended guillotine break at 100% of the cold leg with an area of  $0.456037 \text{ m}^2$ . This is implemented in the simulation by using two trip valves connected to one of the cold legs after the pump discharge line. When the LBLOCA is initiated, flow is directed from the vessel and cold leg to the time-dependent volumes attached to each valve.

The reactor kinetics is handled via the point-kinetics model within RELAP5/MOD3.4. For conservatism, the negative reactivity insertion due to the control rod worth is not taken into consideration according to the APR1400 DCD. Furthermore, an MTC of  $0.9 \times 10^{-4} (\Delta\rho/^\circ\text{C})$  along with the least negative Doppler coefficient used to be consistent with the conservative assumptions adopted in APR1400

DCD. The system is initialized using the nominal operative conditions provided for LOCA in Chapter 15 of APR1400 DCD, which are listed in Table 1.

**2.2. BEPU Approach for Data Generation.** It is necessary to generate a statistically representative database for the training and development of a machine learning metamodel. To this end, the Best Estimate Plus Uncertainty (BEPU) methodology is applied to propagate key uncertain parameters into the thermal-hydraulics model, RELAP5/MOD3.4. The set of key uncertain parameters are derived from the Phenomena Identification and Ranking Table (PIRT) developed for the LBLOCA scenario [28, 30] as listed in Table 2.

To automate this process, an uncertainty quantification (UQ) framework, is developed by loosely coupling the statistical tool, DAKOTA [31], to the thermal-hydraulic system code, RELAP5/MOD3.4, via a Python script. The Monte Carlo (MC) random sampling technique along with the Latin hyper-cube (LHC) method is used to define a combination of input parameters that scan the spectrum of all possible initial and boundary conditions for the thermal-hydraulics model.

The LHC sampling method allows for efficient distribution generation of plausible realizations of values from a multidimensional distribution [54] and was, therefore, used to cover the distribution with fewer samples and hence

TABLE 1: General system parameters and initial conditions.

Parameters	DCD
Power (MWt)	3,983
Power peaking factor	2.258
RCP flowrate (kg/s)	5250.0
Core flowrate (kg/s)	20361.0
Primary pressure (MPa)	15.51
Feedwater temperature (K)	505.23
Safety injection tank coolant volume (m <sup>3</sup> )	52.63
Safety injection tank gas pressure (MPa)	4.25
Safety injection tank coolant temperature (K)	302.5
IRWST temperature (K)	302.5
Core inlet temperature (K)	563.8
Core outlet temperature (K)	597.1
Upper head temperature (K)	584.5
Pressurizer level (m)	8.18
Secondary pressure (MPa)	6.86

reduce the computational burden of conventional MC techniques such as bootstrap [32].

DAKOTA then passes the uncertain parameters to the RELAP5/MOD3.4 code by reading and writing text files in the developed framework. The uncertain parameters are written into the steady state and transient RELAP5/MOD3.4 input files and output files from RELAP5/MOD3.4 calculations are passed back to the DAKOTA results file. A Python script is responsible for the input preparation, data exchange between DAKOTA and RELAP5/MOD3.4, as well as the output postprocessing before passing the sample into the data frame as shown in Figure 3.

**2.3. Machine Learning Metamodel.** In general, there are three main categories of machine learning, namely, supervised learning, unsupervised learning, and reinforcement learning. Supervised learning algorithms are designed to learn by example. The algorithm is given the labelled outputs for a set of inputs. Based on the dataset designated for a machine to learn from, the algorithm can predict the correct answer for the new input data. On the other hand, unsupervised learning does not have labelled data to learn from. Instead, it clusters similar outputs into groups based on common input features. Reinforced learning is based on a reward system. By observing the environment, the algorithm interprets the input and takes an appropriate action in order to be rewarded [33].

In this research, a supervised machine learning technique is implemented. Supervised learning is further divided into the following two categories: classification and regression. Classification is a method where inputs and outputs are classified with labels. The goal of this method is a prediction of single or multiple related binary class labels. This method is well suited for anomaly detection. Regression is similar to classification, but the prediction is performed over a continuous domain. For this reason, regression is well suited for forecasting based on historical time-stamped data [34]. Predicting the future (time series forecasting) such as the stock market price [35] or weather forecasting [36] can be done using a class of artificial neural networks called

recurrent neural networks (RNNs). RNN uses an algorithm called backpropagation through time (BPTT) to look back at historical data using outputs from previous neurons. Using this method, an artificial neuron preserves some state information across time steps in a part of the neural network called a memory cell [37].

A particular problem with RNNs is using short-term memory, hence losing some information at each time step of a long sequence. The other weakness is exposed during training when an error occurs. This error is backpropagated through the entire length of the sequence with the same weights. During each time step, backpropagated gradients may dramatically increase or decrease. Especially in long sequences, this process may lead to gradient diminish or growth at an exponential rate and hence vanish or explode [38, 39]. These phenomena are known as vanishing or exploding gradient problems.

These issues can be mitigated by eliminating the repeat multiplication by the same weight vector during backpropagation in an RNN [39]. This weight correction has been implemented in the long short-term model (LSTM) proposed by Hochreiter and Schmidhuber [40].

The LSTM is specifically designed to control the gradient for a longer duration. In an LSTM cell unit, there are three gates, namely, forget gate, input gate, and output gate, as illustrated in Figure 4. These gates regulate information flow within the cell. The input gate dictates how the activation should be updated in response to the new input. This determines which information is to be stored in the long-term memory and which should be stored in the short-term memory. The output gate dictates which activation should be used, hence determining the hidden states where information about previous inputs is stored. The forget gate determines which data from the previous time step should be passed on and which data should be discarded [42].

Similar to the LSTM unit, the gated recurrent unit (GRU) shown in Figure 5 as proposed by Cho and Bahdanau [43], controls the information flow from the previous time step; but instead of using three cell units GRU uses two, namely, reset gate and update gate [44]. The update gate is responsible for the determination of the amount of previous information that needs to be passed along to the next state. This way the model can decide to copy all information from the past and, therefore, eliminate the risk of vanishing gradient. The reset gate is used to decide how much of the past information should be neglected; basically, it decides whether the previous cell state is important or not.

In an extension of the previous work by Sallehuddin and Diab [28] where an artificial neural network (ANN) was used to predict the maximum value of the peak cladding temperature (PCT) for different initial and boundary conditions, this research is aimed at forecasting the evolution of the PCT over time as the accident progresses. For this class of problems, time-series forecasting based on recurrent neural network (RNN) is the most effective ML tool. Two variations are used for this work, namely, LSTM and GRU. Each uses historical observations (in this case, 5 seconds of simulation time represented by 10 data points) for the prediction of the next data point of the NPP response [45].

TABLE 2: Normalized uncertain parameters [28, 30].

Nos.	Parameter description	Mean, $\mu$	PDF	Standard deviation, $\sigma$	Range, $L_{\text{high}}-L_{\text{low}}$
1	Core power	1.0	Normal	0.0155	0.9691–1.0309
2	Groeneveld-CHF	1.0	Normal	0.500	0.171–2.1711
3	Chen nucleate boiling HTC	1.0	Normal	0.234	0.382–1.618
4	Transition boiling HTC	1.0	Normal	0.230	0.54–1.46
5	Dittus–Boelter liquid HTC	1.0	Normal	0.196	0.607–1.393
6	Dittus–Boelter vapor HTC	1.0	Normal	0.196	0.607–1.393
7	Film boiling HTC	1.0	Normal	0.287	0.426–1.574
8	Break discharge coefficient	1.0	Normal	0.115	0.77–1.23
9	Decay heat	1.0	Normal	0.051	0.898–1.102
10	Oxidization dial	1.0	Normal	0.01	0.980–1.020
11	SIT actuation pressure	1.0	Normal	0.025	0.949–1.051
12	SIT loss coefficient	1.0	Normal	0.20	0.6–1.4
13	Pressurizer pressure	1.0	Normal	0.113	0.77–1.23
14	Fuel thermal conductivity	1.0	Normal	0.0773	0.8455–1.1545
15	Gap conductance	—	Uniform	—	0.75–1.50
16	Downcomer wall thermal conductivity	—	Uniform	—	1.0–2.0
17	SIT water inventory	—	Uniform	—	0.9634–1.0372
18	Pump two-phase head multiplier	—	Uniform	—	0.0–1.0
19	Pump two-phase torque multiplier	—	Uniform	—	0.0–1.0
20	SIT water temperature	—	Uniform	—	0.955–1.045
21	SIP (IRWST) water temperature	—	Uniform	—	0.936–1.064
22	SIP flow multiplier	—	Uniform	—	0.5–1.5
23	Pump K-factor	—	Uniform	—	0.239–0.577

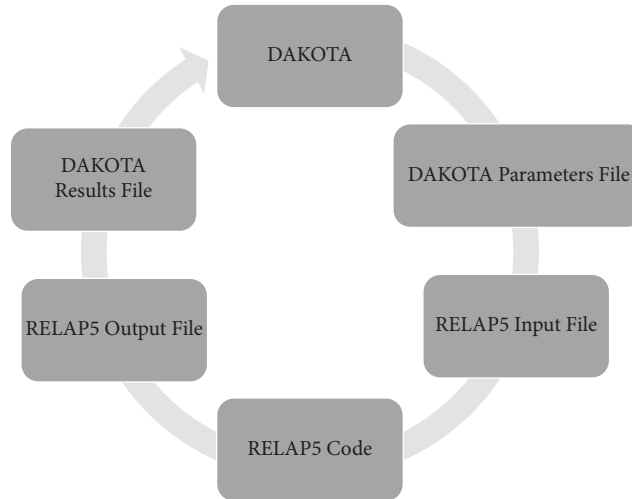


FIGURE 3: Uncertainty propagation framework.

Any ML model is built off of a number of hyperparameters, such as the number of layers, number of neurons per layer, and activation function. A dictionary of all hyperparameters and the search space to be considered is listed in Table 3. During the development of the ML model, these hyperparameters need to be selected and optimized to arrive at the best combination that yields the highest performance.

For the LSTM and GRU models, Talos, the open-source hyperparameter optimization framework developed for Keras models [46] was utilized to automate the optimization process [47, 48]. Various combinations of hyperparameters selected from the provided dictionary are tested within the Talos loop as shown in Figure 6.

### 3. Results and Discussion

This section is dedicated for the presentation and discussion of the results. First, the thermal-hydraulic model predictions for the LBLOCA scenario are discussed. Next, the data generation results from the uncertainty propagation framework followed by data processing and ML model results are presented.

**3.1. Thermal-Hydraulic Model Results.** As mentioned earlier, the thermal-hydraulic model of APR1400 was developed in RELAP5/MOD3.4 based on the parameters and initial conditions reported in APR1400 DCD [49] as listed in

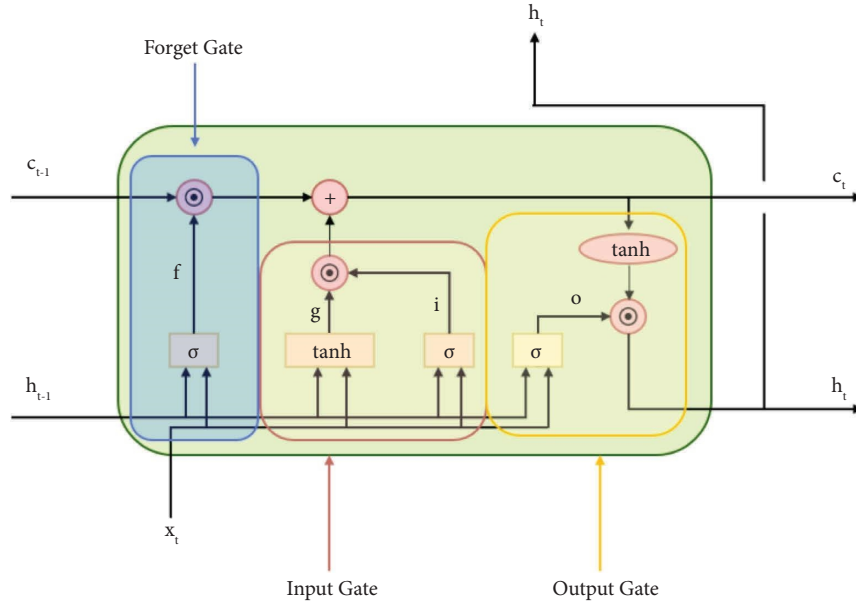


FIGURE 4: Block diagram of the LSTM recurrent network “cell” [41].

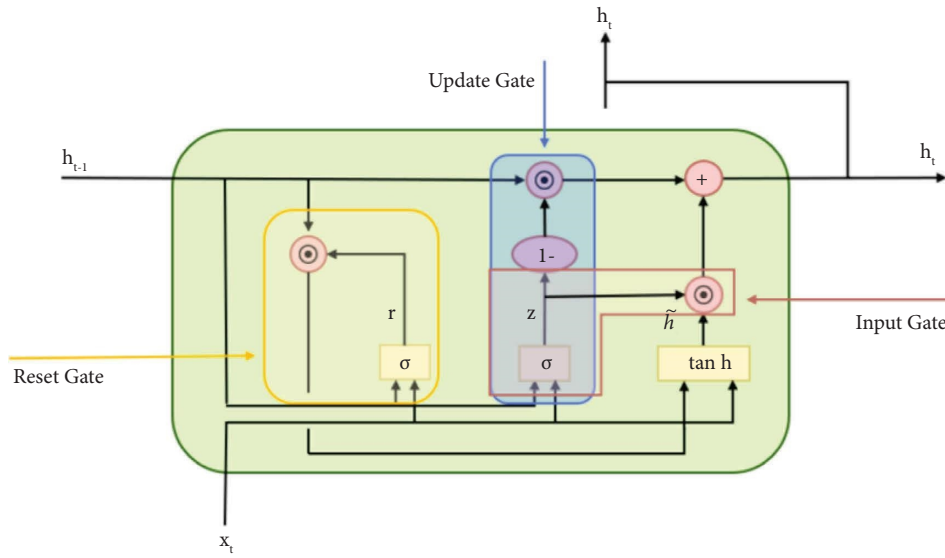


FIGURE 5: Block diagram of the GRU recurrent network “cell” [41].

TABLE 3: Dictionary of hyperparameters.

Hyperparameters	Search space
Number of neurons in 1 <sup>st</sup> layer	13, 25, 50
Number of neurons in a final layer	1
Number of hidden layers	1, 2, 3
Optimizer	Adam, Nadam, SGD, RMSprop
Activation functions	ReLU, Tanh, Sigmoid, Softmax
Recurrent activation functions	Sigmoid, ReLU, Tanh
Dropout	0, 0.1, 0.2
Batch size	64, 100, 200
Number of iterations	15, 20, 35, 40
Kernel regularizers l1	$1 \times 10^{-4}$ , $1 \times 10^{-5}$ , $1 \times 10^{-6}$



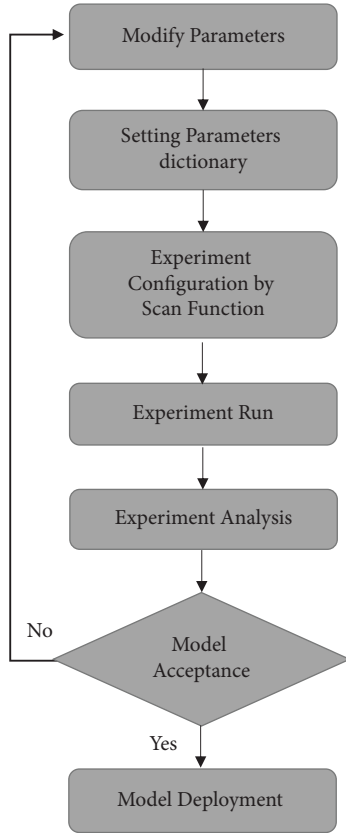


FIGURE 6: Talos optimization process flowchart [9].

TABLE 4: Steady state validation.

Parameters	Model	DCD
Power, (MWt)	3,983	3,983
Power peaking factor	2.2	2.258
RCP flowrate, (kg/s)	5313.5	5250.0
Core flowrate, (kg/s)	20326.2	20361.0
Primary pressure, (MPa)	15.55	15.51
Feedwater temperature, (K)	505.62	505.23
Safety injection tank coolant volume, (m <sup>3</sup> )	52.61	52.63
Safety injection tank gas pressure, (MPa)	4.31	4.25
Safety injection tank coolant temperature, (K)	302.59	302.5
IRWST temperature, (K)	302.45	302.5
Core inlet temperature, (K)	563.93	563.8
Core outlet temperature, (K)	607.5	597.1
Upper head temperature, (K)	563.7	584.5
Pressurizer level, (m)	7.91	8.18
Secondary pressure, (MPa)	6.89	6.86

Table 1 to arrive at a similar nominal steady state condition before the accident is initiated. Table 4 lists the result of validating the steady state response.

Next, the large break loss of coolant accident is initiated by activating the relevant trip valves connected to the cold leg between the pump discharge line and the RPV with an area of 0.456037 m<sup>2</sup> to simulate the double-ended guillotine break. Once the break is initiated, the RCS experiences a rapid pressure drop as the inventory is lost through the break. Flashing causes the coolant to transition from

TABLE 5: Transient validation for key events.

Timing of key events (s)	Model	DCD
Break occurs	0	0
Reactor trip signal occurs	5.8	6.2
SI injection signal occurs	5.8	6.2
SIT discharge begins	16.0	14.4
SIP initiated	48.0	46.2
SIT empty time	204.0	201.5

subcooled to saturation conditions, the collapsed water level drops, and the core uncovers as the RPV becomes voided. The safety injection system (SIS) responds via its four safety injection tanks (SITs) and four safety injection pumps (SIPs). Following the conservative analysis presented in the DCD, one of the emergency diesel generator (EDG) is lost; hence, only two SIPs are available after a 40 sec. time delay; the one near the break and the one across from it on the opposite side. Furthermore, loss of offsite power (LOOP) is assumed, causing the reactor coolant pumps (RCPs) to coastdown. Though the reactor trip signal is initiated at a low RCS pressure signal, the negative reactivity insertion from the control rods are not credited for conservatism. Under these conservative conditions, the generated void should bring the reactor to a shutdown and the safety injection should be enough to cool down the fuel and replenish the inventory. The main events of the transient simulation are compared to those reported in the DCD for validation with reasonable agreement as listed in Table 5.

Upon rupture of the cold leg, the inventory rushes through the break, initially as a liquid until enough inventory is lost to cause a significant and abrupt pressure drop as illustrated by Figure 7 in conjunction with Figure 8. The rapid drop in pressurizer pressure, shown in Figure 8, is a key characteristic of the blowdown phase of the LBLOCA, reflecting the change in the reactor coolant system (RCS) pressure during the transient.

As a result of the blowdown condition initiated by the cold leg break, loss of inventory and rapid depressurization ensue, which causes flashing of the remaining coolant and hence the core starts to uncover. Once uncovered, the core temperature increases as evidenced by the peak cladding temperature (PCT), as shown in Figure 9. This is the maximum cladding temperature observed for the hottest vertical node of the “hot” channel or “average” channel. Due to the deterioration of heat transfer capability of the surrounding vapor phase, the cladding temperature increased to 831.2°C at 10.5 seconds after the break. The PCT predicted by the RELAP5/MOD3.4 model is compared to that reported in DCD with reasonable agreement. According to the DCD, the fuel cladding temperature cannot exceed 1204.44°C. As the results show, this temperature has not been reached, and hence the safety criterion is satisfied.

This temperature increase is halted and the PCT starts to drop as a result of both the decrease in decay heat and the cooling effect provided by the condensate dropping from the upper guide structures (UGSs) and upper head until ~17 seconds. With the depletion of condensate and buildup of decay heat, the cladding temperature starts to increase



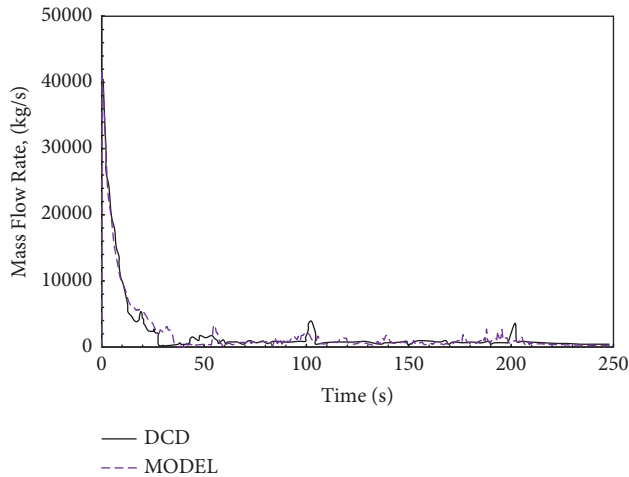


FIGURE 7: Break flow rate.

again until the safety injection system (SIS) is activated and the emergency cooling water starts to fill the downcomer and lower plenum (refill phase) and ultimately refloods the core (reflooding phase).

The emergency cooling water is introduced via four safety injection tanks as well as the two available SIPs on the active train as demonstrated by the SIS flow rate shown in Figure 10. When the system pressure reaches the set point of 4.2 MPa ( $\sim 43 \text{ kg/cm}^2$ ), the emergency cooling water rushes from the safety injection tanks (SITs) into the RCS by gravity at  $\sim 16$  seconds. Given the special design of the fluidic device, the SITs initially provide a very high flow rate with a maximum of  $\sim 700 \text{ kg/s}$  at  $\sim 30$  seconds when the rate of decay heat is highest, it then shifts to a low flow rate (until  $\sim 200$  seconds) as the decay heat drops. In addition, once the system pressure reaches the set point of 12.5 MPa ( $128 \text{ kg/cm}^2$ ), at 48.0 seconds, the SIS initiates SIP injection with a time delay of 40.0 seconds until the pumps start. The depletion of SITs at  $\sim 200$  seconds marks the end of the reflood phase, and the SIPs take over the task of replenishing the core. The emergency core cooling water covers and quenches the core as evident by the drop in PCT (Figure 8).

During the transient, the normalized power increases, reaching 1.65 driven by the moderator temperature feedback mechanism as shown in Figure 11. This is attributed to the cooling effect associated with the rapid depressurization during blowdown with instantaneously very high flow rates in the core as illustrated in Figure 12, which causes the heat transfer coefficient to be very effective momentarily. However, with rapid depressurization and flashing, the core is uncovered and heats up accordingly. This in turn hampers the increase in power due to the Doppler effect.

While the model captures the system response qualitatively well, there are clear deviations between the predicted values and those reported in the DCD. The quantitative differences may be attributed to differences in modelling approach, nodalization, and code options, along with other user effects.

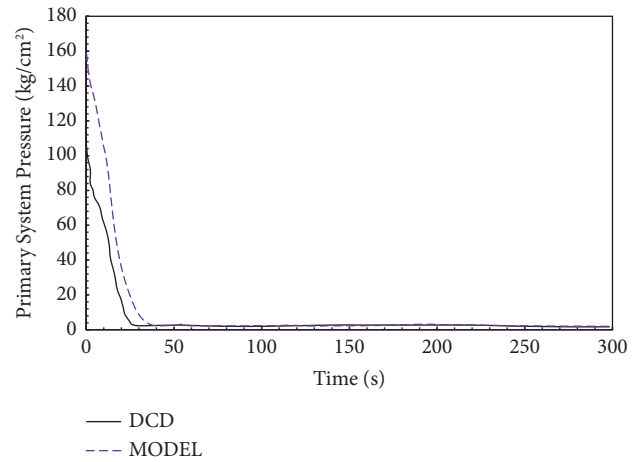


FIGURE 8: Primary system pressure.

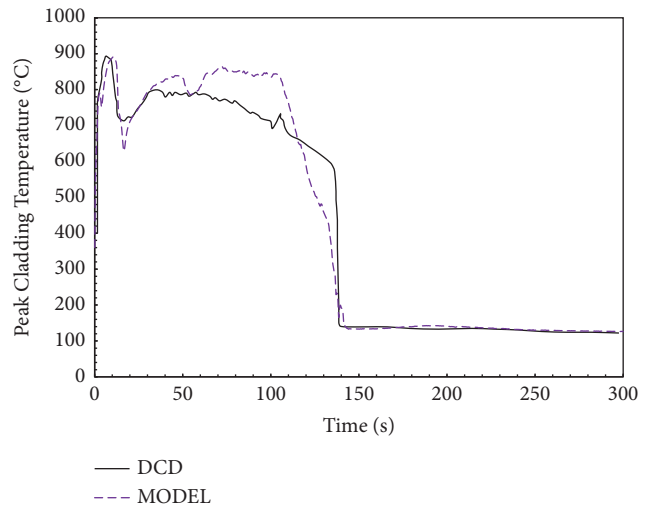


FIGURE 9: Peak cladding temperature.

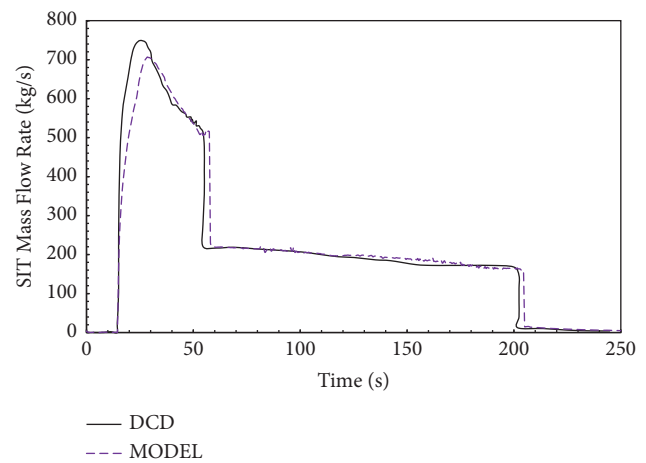


FIGURE 10: SIT mass flow rate.

In DCD, the CAREM methodology is adopted for LOCA analysis, with the RELAP5/MOD3.3 code used for the calculation of ECCS thermal-hydraulics behavior and cladding

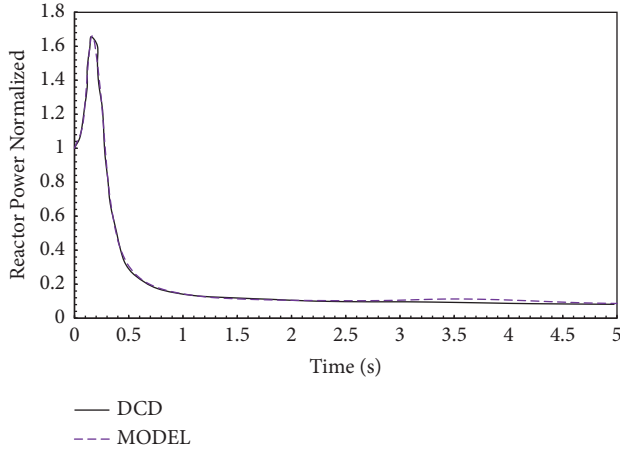


FIGURE 11: Reactor power.

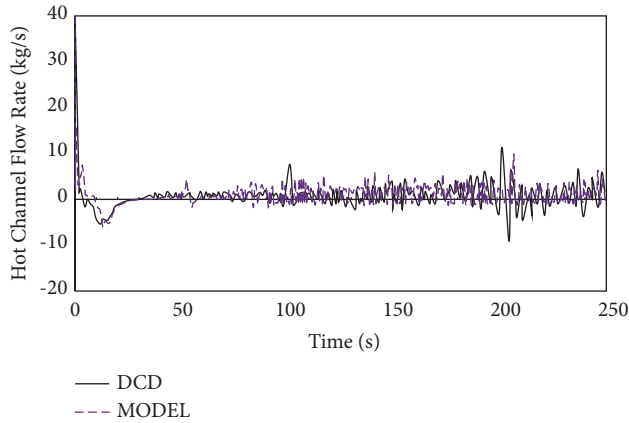


FIGURE 12: Hot assembly mass flow rate.

temperature. In the current work, the best estimate thermal-hydraulic system code, RELAP5/MOD3.4, is used. The RELAP5 code was developed for the best-estimate transient simulation of light-water-reactor coolant systems.

The code has been used worldwide for analyzing large- and small-break LOCAs and operational transients, such as anticipated transient without scram, loss of offsite power, loss of feedwater, and loss of flow. The RELAP5/MOD3.4 code is based on a nonhomogeneous, nonequilibrium model for the two-phase system that is solved by a fast, partially implicit numerical scheme to permit economical calculation of system transients.

In the DCD, the containment back pressure and temperature calculations are performed by the CONTEMPT4/MOD5 code. Due to the mass and energy release rate, the containment back pressure is affected. Simultaneously, the thermal-hydraulics phenomena in the RCS depend on the containment back pressure. Hence, RELAP5/MOD3.3 and CONTEMPT4/MOD5 are coupled together for dynamic data exchange in real time. This is a limitation of the current work since instead of a coupled analysis, the condition in the containment is represented statically using a time dependent volume to reflect the pressure increase associated with the LBLOCA.

Furthermore, when the break flow transitions from subcooled critical flow to saturated critical flow, the magnitude of the break flow will be impacted. For small break analysis, the break flow remains critical and is, therefore, indifferent of the containment condition. However, this may not be true for LBLOCA, and a coupled analysis seems to be indispensable for accurate estimation of the break flow. This is a limitation of the current work; nonetheless, the boundary condition approximation is deemed reasonable since the goal of this work is to develop a machine learning model rather than a details thermal-hydraulic model of LBLOCA.

In addition, the Ransom–Trapp critical flow model is used for the DCD analysis, while in the current simulation, the Henry–Fauske critical flow model is applied. Unfortunately, the Ransom–Trapp critical flow model is not available in RELAP5/MOD3.4. Furthermore, the system nodalization and intricate details such various loss coefficients not published in APR1400 DCD may also contribute to the observed quantitative deviations.

**3.2. Data Postprocessing.** As mentioned earlier, the thermal-hydraulic model prepared in RELAP5/MOD3.4 is fitted with a list of uncertain parameters selected within the provided range and statistical distributions at random using the LHC method along with Wilk’s methodology. Those parameters are passed to the thermal-hydraulic model and run several times within DAKOTA uncertainty quantification framework until a statistically representative sample size is achieved. According to Wilk’s 5<sup>th</sup> order, a sample size of 181 is sufficient; however, it was found that a database in excess of 400 is needed for proper training of the ML model. A database of 450 samples is obtained by DAKOTA, as shown in Figures 13–16. Next, the most probable PCT curve was identified following the USNRC rule [50] of 95% probability and 95% confidence level. To avoid the model overfitting, the sample representing the most probable response was dropped from the training dataset and used for validation of the model at a later stage.

**3.3. ML Model Results.** From a safety perspective, the accuracy of the ML model is most important at the higher end of the range of PCT. Due to the data distribution, the ML model tends to underpredict the upper range of the PCT data regardless of the database size. It is worthy to note that as high as 5746 samples were tested with no avail.

To enhance the prediction accuracy, the oversampling technique was applied by adding 225 samples of the highest PCT values to the original database of 450 samples. Both datasets are mutually exclusive; therefore, there is no chance that samples from the original database exist in the auxiliary database. The intention of this oversampling method is to increase the chances of the model being trained to predict PCT in the upper range of the dataset. The manipulation of the training data distribution to solve the imbalance problem is a well-known practice in the ML environment [51, 52]. The same oversampling database was used to predict SIT mass flow, core power, and RCS pressure.

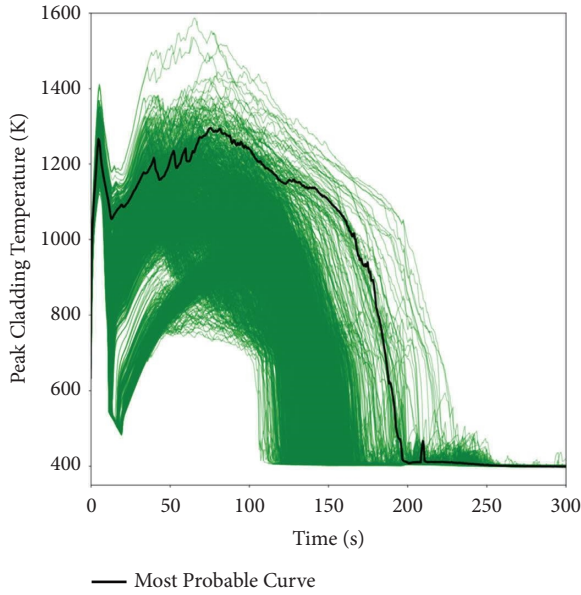


FIGURE 13: PCT database.

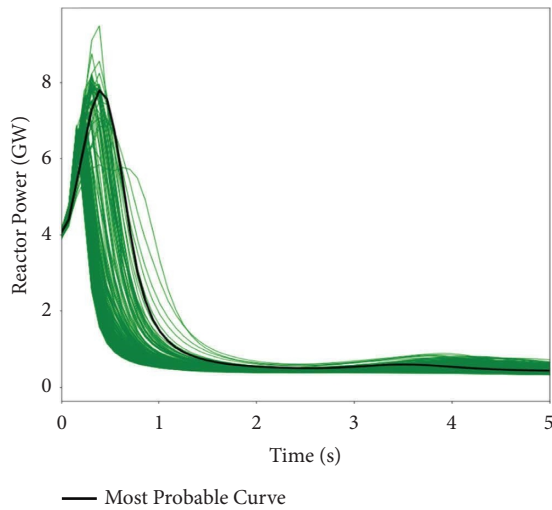


FIGURE 14: Power database.

Before trusting the ML model predictions, validation is indispensable to check that the model is neither overfitting nor underfitting. While underfitting shows that the model is not well trained, overfitting indicates that the trained model is incapable of generalization. To avoid underfitting, the model should be trained on large enough database, and to avoid overfitting, dropout and regularization are usually used to make the model learn more easily, while simultaneously being more capable of generalization and less sensitive to the model weights and number of neurons.

Validation can be achieved by comparing the training and validation loss functions relative to each other. For a fit model, the loss function for both training and validation should converge to a very low value and stay close to each other, with the validation loss slightly larger than that of training.

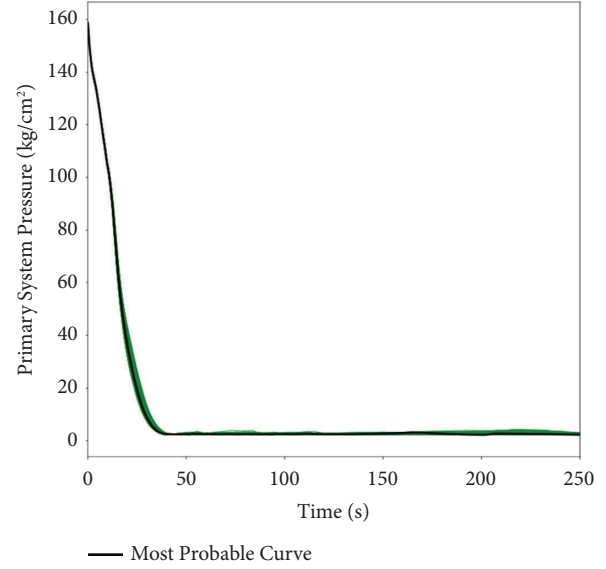


FIGURE 15: Primary system pressure database.

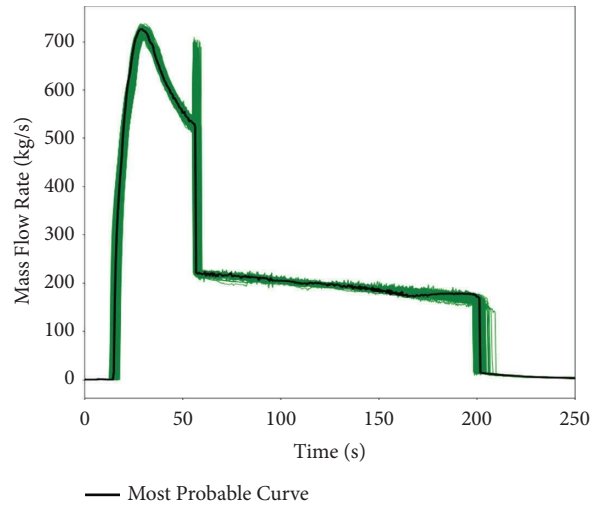


FIGURE 16: SIT database.

To ensure good fitting, it is common practice to split the data at 15%–30%. In this study, 18.3% of the data yields the best validation result. After splitting the data, the model is not exposed to any of the validation data during the training process to prevent overfitting. It is worthy of mention that all models were trained using 20–40 epochs. The training and validation loss are shown in Figures 17–20 for the NPP response predictions. Inspecting those learning curves, the models are deemed to be learning well without experiencing overfitting nor underfitting for the selected hyperparameters listed in Table 6.

After training the different RNN models, they were used to predict the most probable sample. The results of the prediction can be seen in Figures 18–21. The performance of the two RNN models is further assessed by comparing the mean absolute error, mean square error, root mean squared error, and coefficient of determination as listed in Table 7.

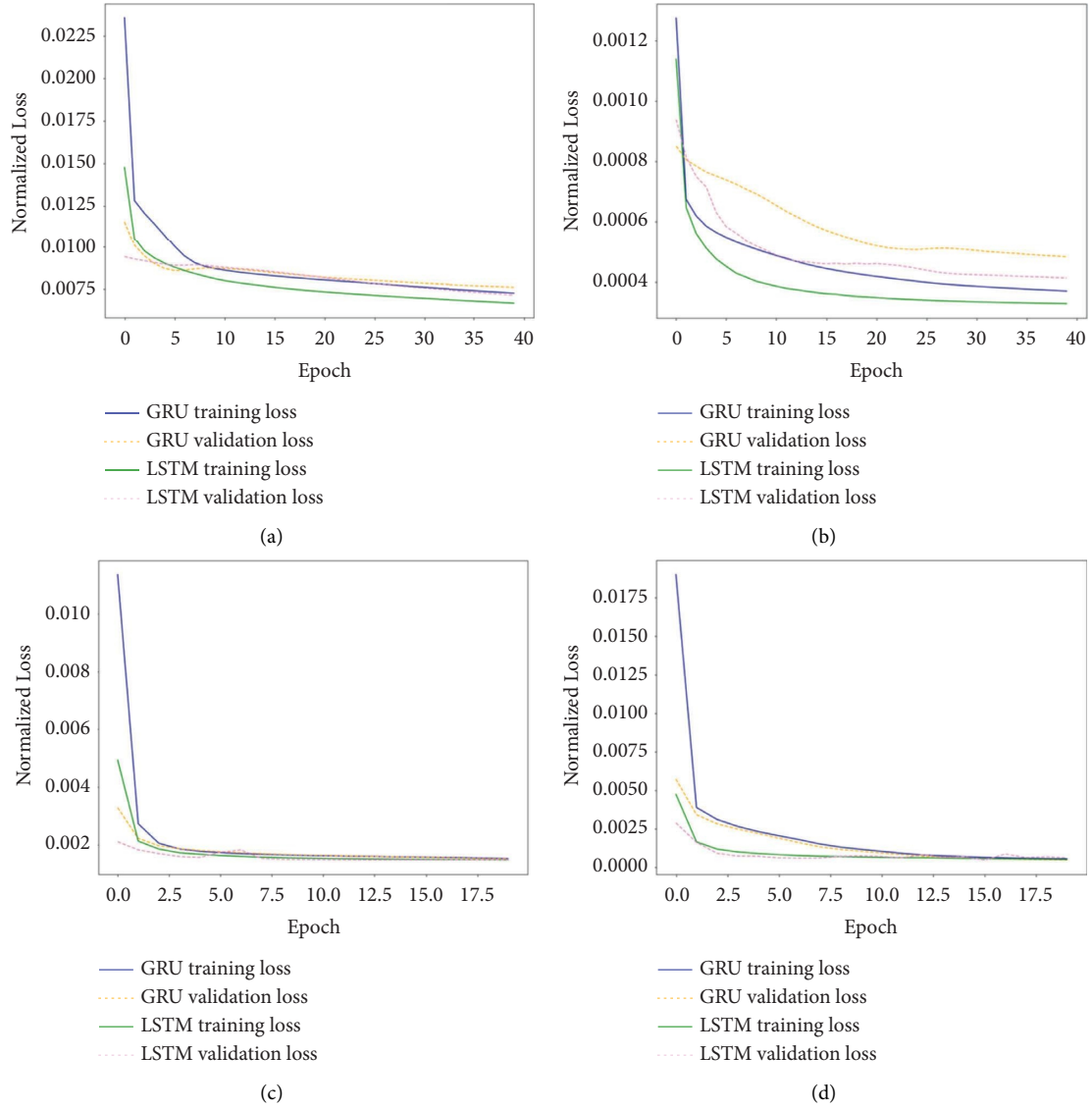


FIGURE 17: Loss function for the key system responses. (a) Peak cladding temperature. (b) Reactor power. (c) Primary system pressure. (d) SIT injection flow rate.

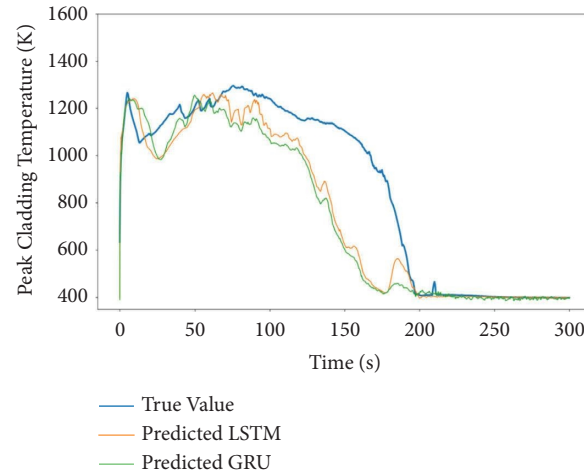


FIGURE 18: ML models prediction of the most probable PCT.

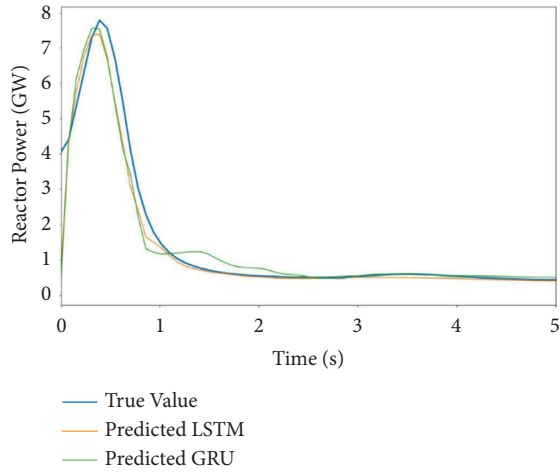


FIGURE 19: ML models prediction of the reactor power.

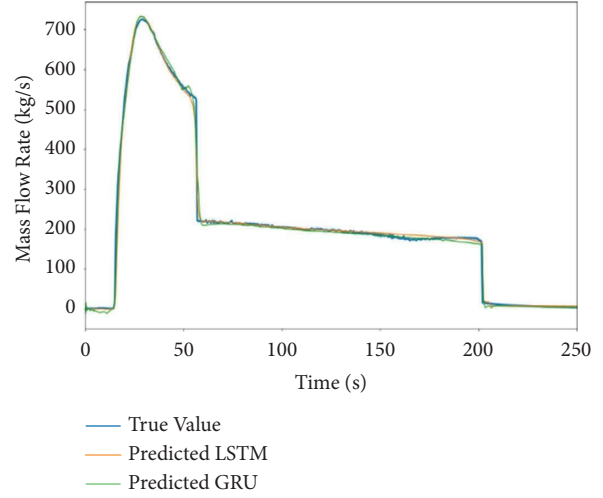


FIGURE 21: ML model prediction of SIT injection.

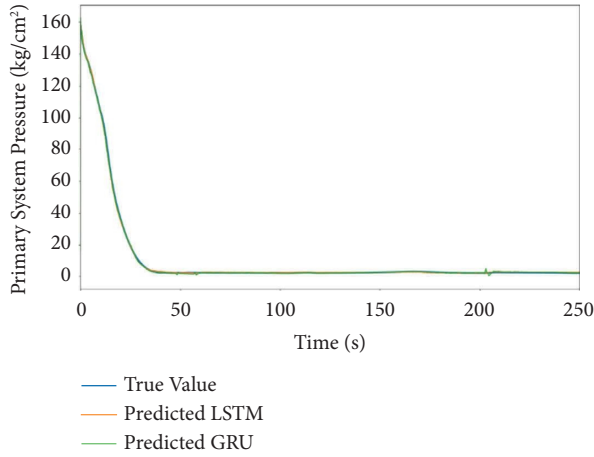


FIGURE 20: ML models prediction of the primary system pressure.

TABLE 6: Selected GRU and LSTM hyperparameters.

Hyperparameters	Value
Number of neurons in 1 <sup>st</sup> layer	13
Number of neurons in a final layer	1
Number of hidden layers	1
Number of neurons in a hidden layer	26
Optimizer	Adam
Activation functions	Tanh, linear
Recurrent activation functions	Relu
Dropout	0
Batch size	64
Number of iterations	20, 40
Kernel regularizer l1	$1 \times 10^{-6}$

Comparing GRU and LSTM models, both have very similar performance. For PCT and power prediction, the LSTM model has better performance than GRU, but GRU has lower errors predicting primary system pressure and SIT mass flow. Both models are predicted with an acceptable amount of error.

TABLE 7: ML model evaluation metrics.

Parameters	ML model	MSE	RMSE	MAE	$R^2$	Accuracy
PCT	GRU	0.002	0.043	0.033	0.983	95.7
	LSTM	0.001	0.036	0.024	0.988	96.4
Pressure	GRU	0.001	0.038	0.007	0.982	96.2
	LSTM	0.002	0.040	0.007	0.980	96
SIT	GRU	0.003	0.018	0.008	0.995	98.2
	LSTM	0.001	0.019	0.006	0.994	98.1
Power	GRU	0.0004	0.020	0.005	0.934	98
	LSTM	0.0004	0.019	0.005	0.940	98.1

## 4. Conclusions

The APR1400 NPP undergoing LBLOCA was modelled using the RELAP5/MOD3.4 thermal-hydraulic system code using the parameters available in the design and control document. The uncertainty propagation (UP) was performed by the DAKOTA uncertainty propagation tool using the Monte Carlo approach along with the Latin hyper-cube method to generate a statistically representative databases and infer the most probable system response. A database of 675 samples including oversampling was used for the prediction of the most probable NPP response for key system parameters, namely: PCT, primary system pressure, SIT mass flow rate, and core power. This work compares two ML models: GRU and LSTM. Both models were tuned to enhance their performance using the Talos hyperparameters optimization tool and later manually adjusted using best engineering practices. The best-performing model with the best loss function characteristic and the lowest error was selected.

Machine learning can be a useful tool for the real-time prediction of critical NPP parameters during accident conditions and can provide operators with useful insight into the decision-making process. The calculations showed that the best-performing LSTM model is capable of

predicting PCT with reasonable accuracy, but for more accurate prediction, a well-balanced dataset is required and the models need further tuning to improve their performance.

With further development, the current work may be used as a cost-effective support tool for the operator. By processing historical data from various instrumentations, it can be used to forecast the time sequence of key system parameters a few seconds forwards into the future. As it stands, it can be used for diagnoses and training but it is intended to expand the machine learning model after training over a spectrum of accident scenarios, so it may be used as an expert system to provide insight for the decision-making involved with operator actions [53–59].

## Data Availability

The data used to support the findings of this study are available from the corresponding author upon request.

## Conflicts of Interest

The authors declare that they have no conflicts of interest.

## Authors' Contributions

Michal Kaminski contributed to methodology, software, validation, formal analysis, data curation, visualization, and writing the original draft. Aya Diab contributed to conceptualization, resources, supervision, analysis, and reviewing and editing. All the authors have read and agreed to the published version of the manuscript.

## Acknowledgments

This research was supported by the 2023 Research Fund of KEPCO International Nuclear Graduate School (KINGS), Ulsan, Republic of Korea.

## References

- [1] J. Bae, G. Kim, and S. J. Lee, "Real-time prediction of nuclear power plant parameter trends following operator actions," *Expert Systems with Applications*, vol. 186, Article ID 115848, 2021.
- [2] L. Hu, Y. Zhang, L. Li, G. H. Su, W. Tian, and S. Qiu, "Investigation of severe accident scenario of PWR response to LOCA along with SBO," *Progress in Nuclear Energy*, vol. 83, pp. 159–166, 2015.
- [3] J. Lee, L. Lin, P. Athe, and N. Dinh, "Development of the machine learning-based safety significant factor inference model for diagnosis in autonomous control system," *Annals of Nuclear Energy*, vol. 162, Article ID 108443, 2021.
- [4] H. Basher and J. S. Neal, *Autonomous Control of Nuclear Power Plants*, Nuclear Science and Technology Division, Maharashtra, India, 2003.
- [5] M. Gomez Fernandez, A. Tokuhito, K. Welter, and Q. Wu, "Nuclear energy system's behavior and decision making using machine learning," *Nuclear Engineering and Design*, vol. 324, pp. 27–34, 2017.
- [6] H. Kim, J. Cho, and J. Park, "Application of a deep learning technique to the development of a fast accident scenario identifier," *Institute of Electrical and Electronics Engineers Access*, vol. 8, pp. 177363–177373, 2020.
- [7] S. Alketbi and A. Diab, "Using artificial intelligence to identify the success window of FLEX strategy under an extended station blackout," *Nuclear Engineering and Design*, vol. 382, Article ID 111368, 2021.
- [8] O. Sharif Sulaiman Alatawneh and A. Diab, "A SE approach to predict the peak cladding temperature using artificial neural network," *Journal of the Korean Society of Systems Engineering*, vol. 16, no. 2, pp. 67–77, 2020.
- [9] O. Sharif Sulaiman Alatawneh, "Prediction of peak cladding temperature using AI for APRI400 under extended station blackout," M.Sc. thesis, KEPCO International Nuclear Graduate School, Ulsan, Korea, 2020.
- [10] W. Sallehudin, S. Al-Ketbi, O. Al-Atawneh, and A. Diab, "Prediction of critical heat flux (CHF) using artificial neural network," 2020, [https://www.researchgate.net/publication/350193129\\_Prediction\\_of\\_Critical\\_Heat\\_Flux\\_CHF\\_Using\\_Artificial\\_Neural\\_Network](https://www.researchgate.net/publication/350193129_Prediction_of_Critical_Heat_Flux_CHF_Using_Artificial_Neural_Network).
- [11] S. K. Moon, W.-P. Baek, and S. H. Chang, "Parametric trends analysis of the critical heat flux based on artificial neural networks," *Nuclear Engineering and Design*, vol. 163, no. 1–2, pp. 29–49, 1996.
- [12] H. Kim, "Prediction of core power distribution using convolutional neural network with ensemble learning," M.Sc. thesis, KEPCO International Nuclear Graduate School, Ulsan, Korea, 2020.
- [13] I. H. Bae, M. G. Na, Y. J. Lee, and G. C. Park, "Calculation of the power peaking factor in a nuclear reactor using support vector regression models," *Annals of Nuclear Energy*, vol. 35, no. 12, pp. 2200–2205, 2008.
- [14] K. Trontl, D. Pevec, and T. Šmuc, "Machine learning of the reactor core loading pattern critical parameters," *Science and Technology of Nuclear Installations*, vol. 2008, Article ID 695153, 6 pages, 2008.
- [15] E. S. Rosa, R. M. Salgado, T. Ohishi, and N. Mastelari, "Performance comparison of artificial neural networks and expert systems applied to flow pattern identification in vertical ascendant gas–liquid flows," *International Journal of Multiphase Flow*, vol. 36, no. 9, pp. 738–754, 2010.
- [16] J. Song and K. Ha, "A simulation and machine learning informed diagnosis of the severe accidents," *Nuclear Engineering and Design*, vol. 395, Article ID 111881, 2022.
- [17] A. A. El-Hameed and J. Kim, "Machine learning-based classification and regression approach for sustainable disaster management: the case study of APRI400 in Korea," *Sustainability*, vol. 13, no. 17, p. 9712, 2021.
- [18] C. M. D. N. A. Pereira, R. Schirru, K. Gomes, and J. L. Cunha, "Artificial neural networks for radiation dose prediction in nuclear emergencies-preliminary investigations," in *Proceedings of the 2016 International Conference on Modeling, Simulation and Optimization Technologies and Applications (MSOTA2016)*, Irvine, CA, USA, January, 2016.
- [19] M. Kimura, S. Aoki, and H. Ohwada, "Predicting radiation protection and toxicity of p53 targeting radioprotectors using machine learning," in *Proceedings of the 2017 IEEE Conference on Computational Intelligence in Bioinformatics and Computational Biology (CIBCB)*, pp. 1–6, Eindhoven, Netherlands, August, 2017.
- [20] J. Iqbal, A. M. Tahir, R. ul Islam, and R. U. Nabi, "Robotics for nuclear power plants— challenges and future perspectives," in *Proceedings of the 2012 2nd International Conference on Applied Robotics for the Power Industry (CARPI)*, pp. 151–156, Zurich, Switzerland, September, 2012.



- [21] J. Iqbal, A. M. Tahir, R. ul Islam, and R. U. Nabi, "Robotics for nuclear power plants— challenges and future perspectives," in *Proceedings of the 2012 2nd International Conference on Applied Robotics for the Power Industry (CARPI)*, pp. 151–156, Zurich, Switzerland, September, 2012.
- [22] J. H. Min, D.-W. Kim, and C.-Y. Park, "Demonstration of the validity of the early warning in online monitoring system for nuclear power plants," *Nuclear Engineering and Design*, vol. 349, pp. 56–62, 2019.
- [23] U. M. Ngbede, "Fault state detection and remaining useful life prediction in AC powered solenoid operated valves based on traditional machine learning and deep neural networks," M.Sc. thesis, KEPCO International Nuclear Graduate School, Ulsan, Korea, 2019.
- [24] H.-K. Jo, "A method to detect anomalies by learning the engine sound during operation of an emergency diesel generator with AI," M.Sc. thesis, KEPCO International Nuclear Graduate School, Ulsan, Korea, 2021.
- [25] F.-C. Chen, M. R. Jahanshahi, and Nb-Cnn, "NB-CNN: deep learning-based crack detection using convolutional neural network and naïve bayes data fusion," *Institute of Electrical and Electronics Engineers Transactions on Industrial Electronics*, vol. 65, no. 5, pp. 4392–4400, 2018.
- [26] M. Boroushaki, M. B. Ghofrani, C. Lucas, and M. J. Yazdanpanah, "Identification and control of a nuclear reactor core (VVER) using recurrent neural networks and fuzzy systems," *Institute of Electrical and Electronics Engineers Transactions on Nuclear Science*, vol. 50, no. 1, pp. 159–174, 2003.
- [27] E. B. Bartlett and R. E. Uhrig, "Nuclear power plant status diagnostics using an artificial neural network," *Nuclear Technology*, vol. 97, no. 3, pp. 272–281, 1992.
- [28] W. Sallehuddin and A. Diab, "Using machine learning to predict the fuel peak cladding temperature for a large break loss of coolant accident," *Frontiers in Energy Research*, vol. 9, 2021.
- [29] M. I. Radaideh, C. Pigg, T. Kozlowski, Y. Deng, and A. Qu, "Neural-based time series forecasting of loss of coolant accidents in nuclear power plants," *Expert Systems with Applications*, vol. 160, Article ID 113699, 2020.
- [30] D. G. Kang, "Analysis of LBLOCA using best estimate plus uncertainties for three-loop nuclear power plant power up-rate," *Annals of Nuclear Energy*, vol. 90, pp. 318–330, 2016.
- [31] B. M. Adams, W. J. Bohnhoff, and K. R. Dalbey, "DAKOTA, A multilevel parallel object-oriented framework for design optimization, parameter estimation, uncertainty quantification, and sensitivity analysis: version 6.9 theory manual," 2020, <https://www.osti.gov/biblio/1630693>.
- [32] J. W. Hines, D. Garvey, and R. Seibert, *Technical Review of On-Line Monitoring Techniques for Performance Assessment: Volume 2 Theoretical Issues*, NRC Contractors, Oak Ridge, TN, USA, 2008.
- [33] T. Sutharssan, S. Stoyanov, C. Bailey, and C. Yin, "Prognostic and health management for engineering systems: a review of the data-driven approach and algorithms," *Journal of Engineering*, vol. 2015, no. 7, pp. 215–222, 2015.
- [34] K. P. Murphy, *Machine Learning: A Probabilistic Perspective*, The MIT Press Massachusetts Institute of Technology, Cambridge, UK, 2012.
- [35] K. Pawar, R. S. Jaleem, and V. Tiwari, "Stock market price prediction using LSTM RNN," *Advances in Intelligent Systems and Computing*, vol. 3, pp. 493–503, 2019.
- [36] A. G. Salman, B. Kanigoro, and Y. Heryadi, "Weather forecasting using deep learning techniques," in *Proceedings of the 2015 International Conference on Advanced Computer Science and Information Systems (ICACSIS)*, pp. 281–285, Depok, Indonesia, October, 2015.
- [37] G. Bronaccorso, *Mastering Machine Learning Algorithms*, Packt Publishing Ltd, Birmingham, UK, 2nd edition, 2020.
- [38] A. Geron, *Hands-On Machine Learning with Scikit-Learn, Keras & TensorFlow Concepts, Tools, and Techniques to Build Intelligent System*, O'Reilly Media, Inc, Sebastopol, CA, USA, 2nd edition, 2019.
- [39] J. D. Kelleher, *Deep Learning*, The MIT Press, Cambridge, UK, 2019.
- [40] S. Hochreiter and J. Schmidhuber, "Long short-term memory," *Neural Computation*, vol. 9, no. 8, pp. 1735–1780, 1997.
- [41] K. I. M. Soohwan, "Sooftware NLP- LSTM & GRU," 2020, [https://sooftware.io/lstm\\_gru/](https://sooftware.io/lstm_gru/).
- [42] I. Goodfellow, Y. Bengio, and A. Courville, *Deep Learning*, The MIT Press, Cambridge, UK, 2016.
- [43] K. Cho, B. V. Merriënboer, C. Gulcehre et al., "Learning phrase representations using RNN encoder-decoder for statistical machine translation," 2014, <https://arxiv.org/abs/1406.1078>.
- [44] Y. Gao and D. Glowacka, "Deep gate recurrent neural network," *Asian Conference on Machine Learning*, PMLR, Montreal, Canada, pp. 350–365, 2016.
- [45] H.-P. Nguyen, J. Liu, and E. Zio, "A long-term prediction approach based on long short-term memory neural networks with automatic parameter optimization by Tree-structured Parzen Estimator and applied to time-series data of NPP steam generators," *Applied Soft Computing*, vol. 89, Article ID 106116, 2020.
- [46] F. Chollet, "Introduction to keras for engineers," 2020, [https://keras.io/getting\\_started/intro\\_to\\_keras\\_for\\_engineers/](https://keras.io/getting_started/intro_to_keras_for_engineers/).
- [47] J. Iqbal, A. M. Tahir, R. ul Islam, and R. U. Nabi, "Robotics for nuclear power plants— challenges and future perspectives," in *Proceedings of the 2012 2nd International Conference on Applied Robotics for the Power Industry (CARPI)*, pp. 151–156, Zurich, Switzerland, September, 2012.
- [48] L. Yang and A. Shami, "On hyperparameter optimization of machine learning algorithms: theory and practice," *Neuro-computing*, vol. 415, pp. 295–316, 2020.
- [49] KEPCO and KHNP, "Apr1400 design control document tier 2 chapter 15 transient and accident analyses," 2013, <https://www.nrc.gov/docs/ML1817/ML18176A051.pdf>.
- [50] USNRC, "USNRC regulatory guide 1.157, best estimate calculation of emergency core cooling system performance," 1989, <https://www.nrc.gov/docs/ML0037/ML003739584.pdf>.
- [51] L. Torgo, R. P. Ribeiro, B. Pfahringer, and P. Branco, "SMOTE for regression," *Progress in Artificial Intelligence*, vol. 8154, pp. 378–389, 2013.
- [52] H. Ahmed, "Regression for imbalanced data with application," 2020, <https://towardsdatascience.com/regression-for-imbalanced-data-with-application-edf93517247c>.
- [53] J. McCarthy, M. L. Minsky, N. Rochester, and C. E. Shannon, *Proposal for the Dartmouth Summer Research Project on Artificial Intelligence*, Dartmouth, Devon, UK, 1955.
- [54] S. J. Russell and P. Norvig, *Artificial Intelligence A Modern Approach*, Pearson Education, Inc, Upper Saddle River, Europe, 2nd edition, 2003.
- [55] A. L. Samuel, "Some studies in machine learning using the game of checkers. II—recent progress," *Indian Bureau of Mines Journal of Research and Development*, vol. 11, no. 6, pp. 601–617, 1967.
- [56] K. Schwab, *The Fourth Industrial Revolution*, World Economic Forum, Geneva, Switzerland, 2016.



- [57] P. Ross and K. Maynard, "Towards a 4th industrial revolution," *Intelligent Buildings International*, vol. 13, no. 3, pp. 159–161, 2021.
- [58] E. Zio, *The Monte Carlo Simulation Method for System Reliability and Risk Analysis*, Springer, London, UK, 2013.
- [59] J. Iqbal, A. M. Tahir, R. ul Islam, and R. U. Nabi, "Robotics for nuclear power plants— challenges and future perspectives," in *Proceedings of the 2012 2nd International Conference on Applied Robotics for the Power Industry (CARPI)*, pp. 151–156, Zurich, Switzerland, September, 2012.